buildings

MDPI

Article

Degradation of Mechanical Performance of Hoop Head Tenon-Mortise Joint of Tusi Manor with Decay Disease in Tibetan Areas in Yunnan

Zhengquan Nong [1], Heng Liu [1], Kua Wu [1], Man Yin [1], Zhe Yuan [2,*], Yanwei Su [1,*] and Mingli Qiang [1,*]

[1] Yunnan Provincial Key Laboratory of Wood Adhesives and Glued Products, Southwest Forestry University, Kunming 650224, China; nzq3719@swfu.edu.cn (Z.N.); liuheng@swfu.edu.cn (H.L.); 2000wk-888@swfu.edu.cn (K.W.); ym196@swfu.edu.cn (M.Y.)
[2] College of Art and Design, Southwest Forestry University, Kunming 650224, China
* Correspondence: yuanzhe@swfu.edu.cn (Z.Y.); suyanwei1218@swfu.edu.cn (Y.S.); qml2889@swfu.edu.cn (M.Q.)

Abstract: (1) The Hoop Head Tenon-mortise Joint (HHTMJ) in the Tusi Manor in Tibetan areas in Yunnan, China, has a serious decay phenomenon. To understand the effect of decay on the seismic performance of HHTMJ, (2) the five groups of HHTMJ and small-size *Pinus kesiya* var. langbianensis wood mechanical property testing specimens were placed in an artificially set decay environment and cultivated together with wood decay fungi for 0, 6, 12, 18, and 24 weeks, respectively. Low-cycle repeated loading tests were conducted to compare the failure mode, hysteresis curve, skeleton curve, and cumulative energy consumption of the HHTMJ under different decay cycles. (3) The results indicate that the failure mode of the HHTMJ is fractured at the tenon shoulder, and the deformation and failure of the tenon increase with the increase in decay. Compared with the non-decayed specimens, the ultimate bearing performance of the specimens after 6, 12, 18, and 24 weeks of decay decreased by 8.83%, 16.97%, 19.69%, and 30.22%, respectively. The cumulative energy consumption decreased by 21.6%, 27.4%, 33.2%, and 41.3%, respectively. (4) Decay primarily occurs on the exterior of the tenon, with minimal decay on the interior. The degradation of seismic performance in HHTMJ is relatively close to the degradation observed in small-size wood specimens during mechanical property testing.

Keywords: Tusi Manor; heritage timber building; Hoop Head Tenon-mortise joint; low-cycle repeated loading; degradation of mechanical properties

check for updates

Citation: Nong, Z.; Liu, H.; Wu, K.; Yin, M.; Yuan, Z.; Su, Y.; Qiang, M. Degradation of Mechanical Performance of Hoop Head Tenon-Mortise Joint of Tusi Manor with Decay Disease in Tibetan Areas in Yunnan. *Buildings* **2024**, *14*, 725. https://doi.org/10.3390/buildings14030725

Academic Editor: Giuseppe Santarsiero

Received: 30 January 2024
Revised: 27 February 2024
Accepted: 4 March 2024
Published: 8 March 2024

Copyright: © 2024 by the authors. Licensee MDPI, Basel, Switzerland. This article is an open access article distributed under the terms and conditions of the Creative Commons Attribution (CC BY) license (https://creativecommons.org/licenses/by/4.0/).

1. Introduction

Wooden frame ancient buildings constitute the primary components of traditional Chinese architecture [1]. In the Tibetan areas of Yunnan, the internal wooden frames of Tusi Manor buildings play a crucial load-bearing role, while the external walls consist of rammed earth, as depicted in Figure 1. The Tibetan areas in Yunnan encompass a typical junction area where various ethnic groups coexist. The local Tusi people preserve Tibetan architectural style while incorporating architectural techniques from other ethnic groups. The Tusi Manor, located at the boundary between high-level halls and ordinary residential areas, represents the culmination of local construction techniques, boasting a rich architectural history and cultural value [2]. The Tibetan areas of Yunnan experience alternating wet and dry climates. Consequently, the original wooden components within the existing Tusi Manor are prone to cracking, insect infestation, and fungal decay. These factors pose a threat to the longevity of the wooden frames [3–5].

The vertical connection between the wooden beams and columns of the Tusi Manor in Tibetan areas of Yunnan primarily relies on the overlay of beams and columns method. Additionally, wooden nails are used to reinforce and connect the beams and columns [6]. For

horizontal connections, Dovetail tenon, Straight Mortise-and-Tenon Joints, and Hoop Head Tenon-mortise Joints (HHTMJ) are primarily used. The HHTMJ connection is specifically employed for connecting the center beam and side column structures. In this type of connection, the tenon shoulder and the mortise and tenon, located outside the wood column, exert mutual pressure, thereby enhancing resistance against compression and pull-out forces. It is considered a special type of mortise and tenon joint [7]. However, due to the frequent exposure of the HHTMJ to the external environment, it is prone to fungal decay. In recent years, scholars have conducted numerous experimental studies to investigate the effects of salvage and disease on the mechanical properties of wood structural joints. For instance, Zhang et al. simulated the degradation of mortise and tenon joints by altering their size and controlling the width of the compression zone and gap [8–11]. King et al. simulated fungal decay, cracking, and degradation of wooden member joints by drilling holes and grooves. They found that degraded joints were susceptible to fungal decay, cracking, and reduced mechanical properties [12,13]. Chen et al. examined the effects of different beam section heights, column diameters, and column top pressures on the mechanical properties of HHTMJ. They also analyzed the moment-rotation relationship of the joints [14,15]. While the above research methods simulated the appearance and mechanical properties of decayed joints, it is important to note that the timber properties of the wood used in these studies did not change and may differ from the actual situation.

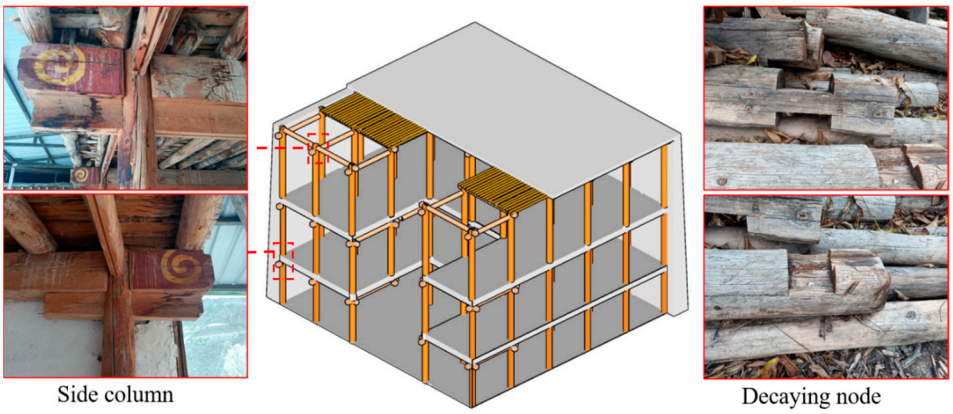


Figure 1. Hoop Head Tenon-mortise Joint used in Tusi Manor.

To study the effect of decay on the degradation of mechanical properties of wood, scholars have conducted a series of studies in the past [16–20], and it was found that the degradation of the mechanical properties of decayed wood was directly proportional to the decay cycle, and many of the mechanical properties of the wood degraded significantly after treatment with a shorter decay cycle, but the majority of these studies were carried out through the decay test of small test specimens. Wang and García, among others, investigated the degradation patterns of the mechanical properties of wood under different artificial decay treatment methods [21,22]. Mi, Yang, and colleagues directly tested the mechanical properties of degraded wood obtained from ancient buildings. They found that, compared to non-degraded specimens, samples removed from ancient buildings exhibited varying degrees of uniform degradation, with aged specimens being more prone to decay [5,23].

Although the mechanical performance derived from small-scale wood specimens can, to some extent, reflect the mechanical properties of full-scale wood components, there may be significant differences in the degradation patterns between small-scale specimens and full-scale specimens when mechanical performance deteriorates [24]. Kim believed that the strength degradation law obtained from the decay test of small specimens did not apply to full-size specimens and conducted decay tests on full-size southern pine specimens and found that the mechanical properties of full-size specimens had been significantly degraded at a lower decay level [25]. To investigate the impact of wood degradation in the

materials used for wooden components on the mechanical performance degradation of these components. Lydia, Zhang, and others conducted damage treatments on wooden components by designing extreme climatic conditions and improving laboratory decay methods. This simulated the mechanical performance degradation of wooden components in real decay environments [26–28]. Ma and Chen et al. conducted experimental research on the removal of damaged mortise and tenon joints from ancient wooden structures and found that as the degree of damage increased, the mechanical properties of the joints decreased significantly [29,30]. The research conducted by these scholars further revealed the mechanical performance of wooden components in timber structures after experiencing degradation. Despite scholars employing various methods over the past decade to simulate decay in HHTMJ, there are still notable differences between these simulation approaches and the actual decay experienced by HHTMJ in practice.

Some researchers have also investigated the degradation of small-sized wood specimens to infer the degradation of full-sized specimens' mechanical properties due to decay. However, owing to the presence of size effects, there are considerable distinctions between the degradation patterns of small-sized specimens and those of full-sized specimens.

To delve into the impact of decay on the mechanical properties and degradation of HHTMJ, we referred to established wood decay standards and methodologies employed by contemporary scholars. Utilizing *Pinus kesiya* var. langbianensis sourced from the Tusi Manor in Tibetan areas of Yunnan as our experimental material, we fashioned a typical HHTMJ specimen representative of the Tusi Manor's structures. By introducing wood-rotting fungi through inoculation, we obtained HHTMJ specimens exhibiting varying degrees of decay specific to the Tusi Manor's buildings in Tibetan areas of Yunnan. Low-cycle repeated loading was employed to subject HHTMJ to loading, investigating the seismic performance of HHTMJ under various degrees of decay. The mechanical properties of *Pinus kesiya* var. langbianensis were also assessed both pre- and post-decay, allowing us to elucidate the degradation of mechanical properties in HHTMJ. We aim to furnish a reference framework for reinforcing and repairing the buildings of the Tusi Manor in the Tibetan areas of Yunnan.

2. Materials and Methods

2.1. HHTMJ Specimen

HHTMJ is crafted from *Pinus kesiya* var. langbianensis, a wood commonly employed in the ancient architecture of Tibetan areas in Yunnan. The average air-dry density of *Pinus kesiya* var. langbianensis was measured at 0.452 g/cm^3, with an average moisture content of 13.3%. To determine the size of the HHTMJ used in this experiment, we referred to the HHTMJ in a Tusi Manor in the Tibetan areas of Yunnan. The column has a length of 1400 mm, a cross-sectional diameter of 200 mm, a beam section height of 160 mm, and a thickness of 60 mm, as illustrated in Figure 2. We designated the number of non-decayed specimens as ST-1 and specimens aged 6 to 24 weeks as ST-2 to ST-5.

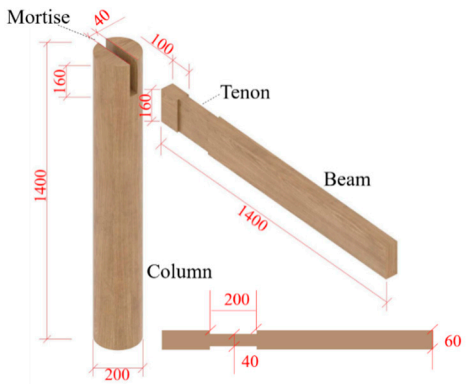


Figure 2. Hoop Head Tenon-mortise Joint.

2.2. Mechanical Properties Testing Specimens

To determine the changes in the mechanical properties of *Pinus kesiya* var. langbianensis before and after decay, a total of 180 specimens were made according to the requirements of the standard [31–34]. These included 30 tensile specimens, compression specimens, and bending and elastic modulus specimens. These small specimens will be subjected to wood rot, fungus decay, and treatment.

During the stress process of mortise and tenon joints, external forces cause significant lateral deformation of the wood at the mortise and tenon joints, while wood parallel to the grain direction hardly deforms [35,36]. To clarify the internal decay of the tenon and minimize differences in mechanical properties among specimens from various parts of *Pinus kesiya* var. langbianensis, we removed one end of the beam that had not undergone decay treatment before initiating decay operations. This severed end functions as a control group, while the other end undergoes decay treatment to assess the occurrence of decay within the tenon. Upon reaching the corresponding decay cycle, we cut the tenon of the HHTMJ after decay treatment into a specimen to examine the extent of degradation in the transverse radial compressive strength of the tenon. Subsequently, we sectioned it into a transverse radial compressive strength test specimen based on the distance from the outer surface, employing the sawing method depicted in Figure 3.

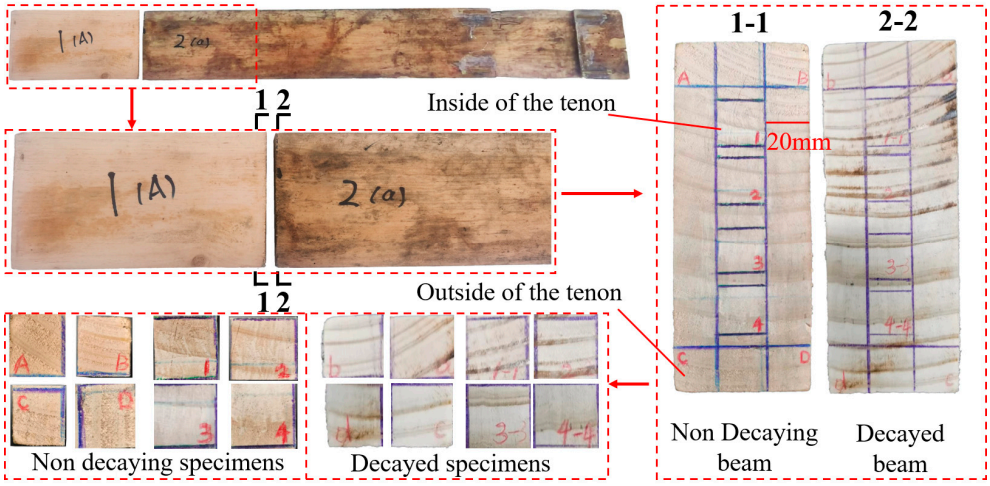


Figure 3. Sampling diagram of tenon decay depth verification specimen. (1-1) Cross section of non-decayed tenon; (2-2) Cross section of decayed tenon.

2.3. Decay Method

The brown rot fungus (strain No. CFCC86617) procured from the China Forestry Microbial Collection Center (CFMC) was selected as the test strain, which is a common decaying fungus in the ancient wooden structures in northwest Yunnan [37]. According to GB/T 13942.1-2009, "wood durability performance Part 1: natural decay resistance laboratory test methods" [38] to expand the culture of brown rot bacteria. Due to the large size of the HHTMJ specimen used, it was not possible to select glassware as the container for the decay test according to the requirements of the standard [38]. Based on the methods provided in the literature [39,40], a wooden box was selected as the outer shell, and a polyethylene bag was selected as the inner liner to simulate the natural decay environment. Soil was placed at the bottom of the polyethylene bag, and feeding wood inoculated with brown rot fungi was placed above the soil. To obtain a more comprehensive brown rot fungus erosion of the tenon, the test piece was brought into contact with the feeding wood, and the small-size mechanical properties testing sample with a culture medium was evenly placed next to the tenon, as shown in Figure 4. Polyethylene bags containing inoculated test samples were then placed in an airtight wooden box, with vents retained to ensure adequate oxygen supply. A sprayer was regularly used to humidify the space every day, maintaining a high humidity level and thereby accelerating the decay

process of the test piece. To determine the humidity in the environment, a temperature and humidity meter is placed next to the decaying tenon. The temperature and humidity meter show that the ambient temperature is around 25 °C and the humidity exceeds 93% within 2 days after humidification of the enclosed space. During the subsequent decay process, the environmental humidity remained above 90%. The environmental temperature and humidity are suitable for the growth of wood rot fungi. When the decay treatment reaches the corresponding cycle, the sample is taken out of a high-humidity environment, as shown in Figure 4. It can be found that the degree of color change and bacterial growth in various areas of the surface of all specimens are the same within the same decay cycle.



Figure 4. Cultivation process of wood rot fungi on test specimens.

2.4. Mechanical Properties of Wood

Gently scrape off the mycelium and debris on the surface of the specimen and place it in a constant temperature and humidity box. Set the temperature to 22 °C and the humidity to 65%, and maintain the equilibrium time for 7 days to maintain the moisture content of the specimen at around 12%. The mechanical properties of the specimen were tested using an electronic universal mechanical testing machine controlled by a microcomputer, as shown in Figure 5. The obtained results are presented in Table 1. The mass loss rate of dry specimens is commonly utilized as an indicator for detecting wood decay [41]. According to the data in Table 1, it can be observed that the weight loss rate of *Pinus kesiya* var. langbianensis is directly proportional to the duration of decay within a 24 week period. The coefficient of variation (COV) represents the level of dispersion in the test data. With a longer decay cycle, there is increased randomness in the location and extent of decay, leading to a higher degree of dispersion in the test data.

After the transverse radial compressive strength test specimens obtained from decayed beams and nondecayed beams, it was found that the compressive strength of the transverse radial inside the tenon did not decrease significantly, indicating a decay cycle of 24 weeks. This indicates that decay mainly occurs on the outer side of the tenon and has little impact on the inner side. At the same time, it was found that the transverse radial compressive strength of the pre-made transverse radial compressive strength test specimen was compared with that of the specimens obtained from the outside of the decayed beam. The degradation level of specimens obtained from the outer side of the decayed beam is less than that of the prefabricated transverse radial compressive strength test specimen. This difference is mainly related to the distance of the wood in the test area from direct exposure to the decay environment.

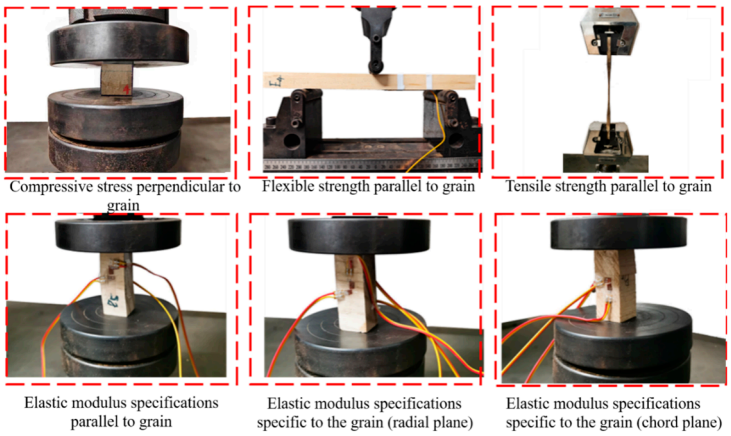


Figure 5. Testing of mechanical properties of Rotten *Pinus kesiya* var. langbianensis.

Table 1. Mechanical properties of *Rotten Pinus* kesiya var. langbianensis.

Mechanical Property/COV Decreased Percentage (%)	Culture Time (Week)				
	0	6	12	18	24
Compressive stress perpendicular to grain (f_{cno}/NDO) (MPa)	3.36/16.2	3.27/12.3	3.46/12.6	3.46/17.6	3.30/14.6
Compressive stress perpendicular to grain (f_{co}/DO) (MPa)	3.35/18.21 0.3%	3.12/25.32 4.6%	3.19/22.4 7.9%	2.97/22.4 13.9%	2.69/24.1 18.4%
Compressive stress perpendicular to grain (f_{cni}/NDI) (MPa)	3.36/19.3	3.33/12.3	3.48/14.7	3.47/15.3	3.32/14.4
Compressive stress perpendicular to grain (f_{ci}/DI) (MPa)	3.36/21.22 0%	3.33/14.5 0%	3.48/15.6 0%	3.46/13.9 0.3%	3.30/15.8 0.6%
Compressive stress perpendicular to grain (f_c/MPa)	3.42/13.3 0.0%	3.03/14.9 11.3%	2.79/13.4 18.4%	2.40/9.8 29.8%	2.27/16.6 33.6%
Flexible strength parallel to grain (MPa)	76.14/16.6 0.0%	61.13/15.60 19.7%	59.04/12.53 22.4%	57.71/22.33 24.2%	45.98/21.6 39.6%
Tensile strength parallel to grain (MPa)	59.71/7.44 0.0%	45.61/15.55 23.6%	43.52/17.53 27.1%	34.87/23.12 41.6%	31.88/30.12 46.6%
Elastic modulus specifications parallel to grain (MPa)	9156/6.41 0.0%	8744/7.22 4.5%	8208/9.60 10.3%	7864/9.62 14.1%	7770/10.8 15.1%
Elastic modulus specifications specific to the grain (radial plane (MPa)	693/7.8 0.0%	679/9.1 2.2%	656/8.9 5.3%	640/11.3 7.6%	615/13.3 11.3%
Elastic modulus specifications specific to the grain (chord plane (MPa)	534/9.2 0.0%	498/10.5 6.7%	451/10.9 15.5%	444/16.3 16.9%	441/17.9 17.4%
Mass loss (%)	55.84/12.3 0.0%	54.6/19.7 2.2%	52.29/22.6 6.4%	50.67/21.3 9.3%	49.53/24.63 11.3%

In the table, NDO represents the transverse radial compressive strength test specimen of the non-decayed external specimen used as a control group on the tenon, DO represents the decayed external specimen, NDI represents the non-decayed internal specimen, and DI represents the decayed internal specimen.

2.5. HHMTJ Loading Device and Method

To prevent the beam from experiencing the P-Δ effect during vertical loading. Simultaneously facilitating the loading and recording of experimental phenomena. As shown in Figure 6, place the column horizontally and apply a horizontal cyclic load at the end of the cantilever beam using an actuator. The connection between the loading point of the actuator and the beam is connected by a spherical hinge support, which is loaded at a distance of 500 mm from the surface of the column. To prevent lateral displacement and instability of the node specimen during loading, the column base of the column is fixed on

the base, and a hydraulic jack is used to apply an axial load of about 20 KN in the Wooden pad axis direction. Steel rings and lower steel plates are used in the middle of the column for bolt fixation. When the actuator is loaded to the right end, it is specified to be loaded in a forward direction, and when loaded to the left end, it is specified to be loaded in a negative direction. The load and horizontal displacement of the loading point are obtained using an actuator sensor.

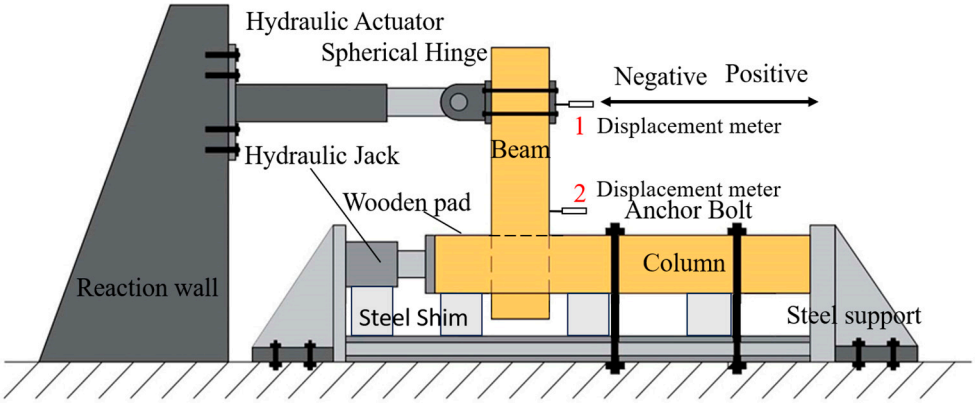


Figure 6. Loading device and measurement point.

The low cycle repeated loading test refers to the provisions of JGJ/T 101-2015 "Code for Seismic Testing of Buildings" [42], and adopts displacement control-graded loading. To control the single loading before the yield section, the first three levels of loading are cycled once with an amplitude of 5 mm. After the completion of the third level of loading, the displacement of each level increases by 5 mm, and each level is cycled 3 times. When the load on the actuator decreases significantly or the node is damaged, the loading is stopped. The loading system is shown in Figure 7.

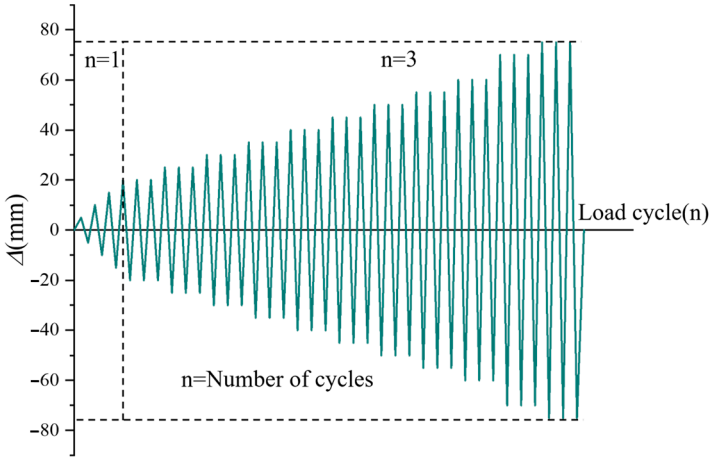


Figure 7. Loading protocol.

3. Results and Analysis

3.1. Failure Mode

For the non-decayed specimen ST-1, during the initial loading stage, small clearances between the joints result in a relatively slow increase in load on the actuator. As loading continues, the tenon and mortise rub against each other, producing slight sounds. After unloading, no significant deformation of the projecting tenon or mortise is observed. When loaded to a displacement of 55 mm, mutual compression between the tenon and mortise leads to increased deformation of the tenon, accompanied by slight cracking sounds at the mortise with wood fibers. Upon further loading to a displacement of 75 mm, distinct

wood fracture sounds are heard at the tenon, cracks form at the tenon shoulder, and the tenon exhibits noticeable plastic deformation and pullout, as shown in Figure 8a. Loading is then stopped.

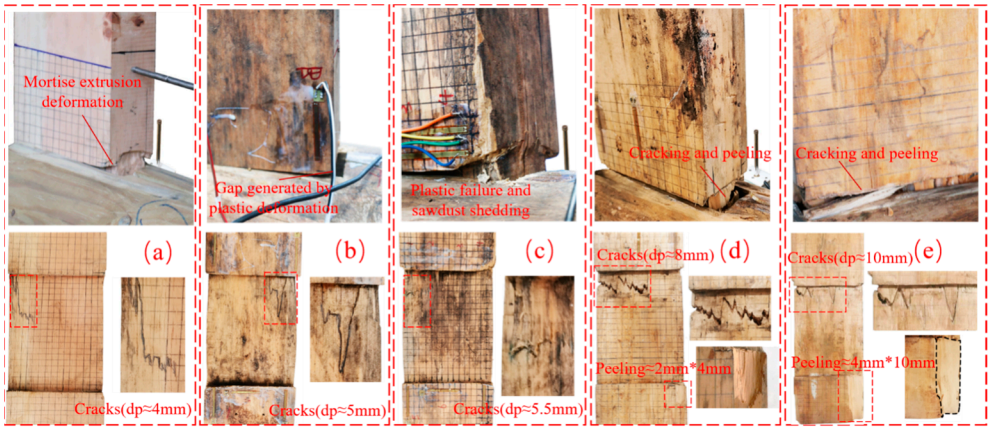


Figure 8. Failure mode of Tenon. (**a**) Deformation and fracture of specimen SJ-1; (**b**) Deformation and fracture of specimen SJ-2; (**c**) Deformation and detachment of tenon joint of specimen SJ-3; (**d**) Cracking and detachment of the tenon joint of specimen SJ-4; (**e**) Cracking and detachment of the tenon joint of specimen SJ-5.

For specimen ST-2, initially, during loading, there was minor plastic deformation in the contact area between the tenon shoulder and the mortise. As loading progressed, the friction and extrusion sounds between the tenon and mortise increased gradually, accompanied by a rise in tenon slip and deformation. When the loading displacement reached 70 mm, a noticeable wood fracture sound was heard at the joint, accompanied by a higher tenon pulling force. Further loading to 75 mm resulted in increased tenon cracks and evident deformation damage at the joint between the tenon shoulder and mortise, as depicted in Figure 8b. Loading was then halted. Like specimen ST-2, specimen ST-3 also showed plastic deformation in the contact area between the tenon shoulder and the mortise at the start of loading. At a displacement of approximately 65 mm, the tenon emitted a small wood-breaking sound, and wood chips dislodged from the shoulder and mortise extrusion area. This was accompanied by a notable tenon pull-out phenomenon, as illustrated in Figure 8c. With continued loading, the plastic deformation became more pronounced. When the loading displacement reached 75 mm, wood chips were shed at the tenon shoulder, and there was evident plastic deformation and damage at the joint. Loading was then stopped.

For specimens ST-4 and ST-5, similar to specimen ST-3, slight plastic deformation and wood chips were shedding at the tenon shoulder during the initial loading. At a loading displacement of 50 mm, specimen ST-4 experienced a notable release of wood chips from the tenon shoulder. When the loading displacement reached 65 mm, the tenon emitted a small sound of wood breaking, and at a continued displacement of 70 mm, a substantial fracture occurred in the tenon. Upon loading to a displacement of 75 mm, the tenon displayed severe plastic deformation and damage, leading to the cessation of loading. The characteristics of node damage are illustrated in Figure 8d. For specimen ST-5, when loaded to 45 mm, a smaller wood fracture sound occurred at the tenon, and the crack gradually expanded with the increasing loading displacement. At a loading displacement of 60 mm, the wood pieces at the tenon shoulder of specimen ST-5 detached in one piece along the grain direction, accompanied by a slight wood fracture sound at the tenon during forward loading. By the time the load reached 70 mm, the tenon emitted a loud sound indicating wood fracture, and visible cracks appeared at the tenon. The actuator showed a significant decrease in load value. Continuing to a load of 75 mm, the actuator load remained nearly unchanged, while the tenon was destroyed. Loading was promptly halted, and the failure characteristics of the node are depicted in Figure 8e. A comprehensive

analysis of the information reveals that with the increase in the decay period, the primary failure mode of HHTMJ under the same load level has not undergone significant changes, mainly displaying fracture failure at the tenon shoulder. However, the extent of damage is increasing, and the failure mode is becoming more complex.

As shown in Figure 9, during positive loading, there is an upward sliding component force on the wood pad at the tenon shoulder, resulting in a tendency for both the stigma and the wood pad to slide upward, whereas during negative loading, there is a downward sliding component force on the wood pad at the tenon shoulder and a tendency for the mortise to slide downward. This makes the nodal bending moment in negative loading greater than that in positive loading. According to the research by Chang [13] et al. on HHTMJ with different degrees of damage, it was found that the phenomenon of relative slippage between the tenon eye and the wood pad would form a "pseudo-dovetail" mechanism in timber frame structures. This mechanism can provide lateral support for the timber frame, and an increase in the degree of damage weakens this mechanism. The damage pattern of the mortise is shown in Figure 10. The degree of damage at the end in contact with the wooden pad is greater than that at the end away from the wooden pad. By comparing the damage characteristics of the mortise and tenon at nodes with different decay cycles, the deformation and splitting phenomena of the head timber are more obvious with the increase in decay cycles.



Figure 9. Movement between column head and wooden cushion block.

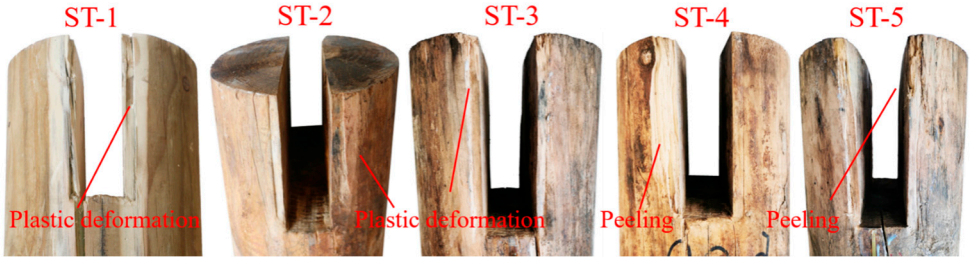


Figure 10. Failure modes of mortise.

Figure 11 illustrates the forces acting on the HHTMJ during forward loading, providing insight into the compressive plastic deformation of the transverse wood grain in the primary compression area of the tenon and mortise. To facilitate the description, designate the primary contact region between the tenon and mortise as point ABCD. When force F is applied, the cross-grain direction of the tenon at points A and D undergoes compression by the cross-grain direction of the mortise, resulting in plastic deformation. Similarly, the wood at the tenon's shoulder is extruded in the cross-grain direction by the wood of the extrusion post, with the extrusion depth increasing along the midpoint of the dotted line on both sides.

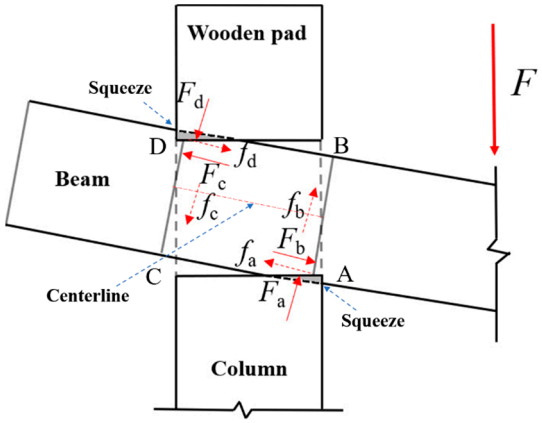


Figure 11. Mechanical deformation of HHTMJ.

Figure 12 presents the stress analysis of the HHTMJ cross-section, shedding light on the occurrence of wood chip-off at the tenon shoulder and extrusion deformation of the wood at the mortise edge during larger loading displacements. During negative loading, the post head applies force F_b to the tenon shoulder. Referring to Figure 11 makes it evident that stresses become more concentrated the farther they are from the tenon center. This concentration leads to increased susceptibility of the wood at the edge of the tenon shoulder to plastic deformation. In the case of forward loading, the wood size at the CD end of the HHTMJ tenon is smaller. The tenon shoulder's edge is prone to plastic deformation when subjected to the concentrated force F_c. The tenon shoulder generates significant paragrain shear stress, and the wood paragrain shear strength decreases with a large decay cycle and a small length lc of the upper end of the tenon. This reduced paragrain shear resistance contributes to the woodshedding at the edge of the tenon shoulder in the paragrain direction.

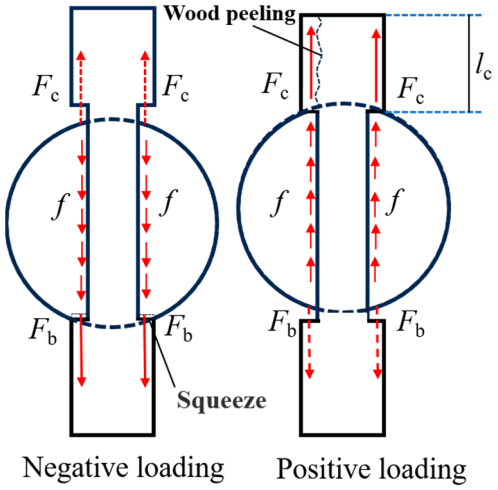


Figure 12. Stress analysis of specimen cross section.

3.2. Hysteresis Curve and Skeleton Curve

The *M*-*θ* hysteresis curve under horizontal low-cycle cyclic load can describe the seismic performance of mortise-tenon joints. The larger the area enclosed by the hysteresis loop, the stronger the energy dissipation capacity of the joints and the better the seismic performance. The bending moment (M) and its corresponding turning angle (θ) are determined as follows:

$$M = PH \tag{1}$$

$$\theta = \Delta / H \tag{2}$$

where P is the load applied by the actuator, H is the distance between the upper surface of the column and the loading. point, and Δ is the horizontal displacement of the loading point. Figure 13 demonstrates the hysteresis curve and skeleton curve of the HHTMJ in this experiment.

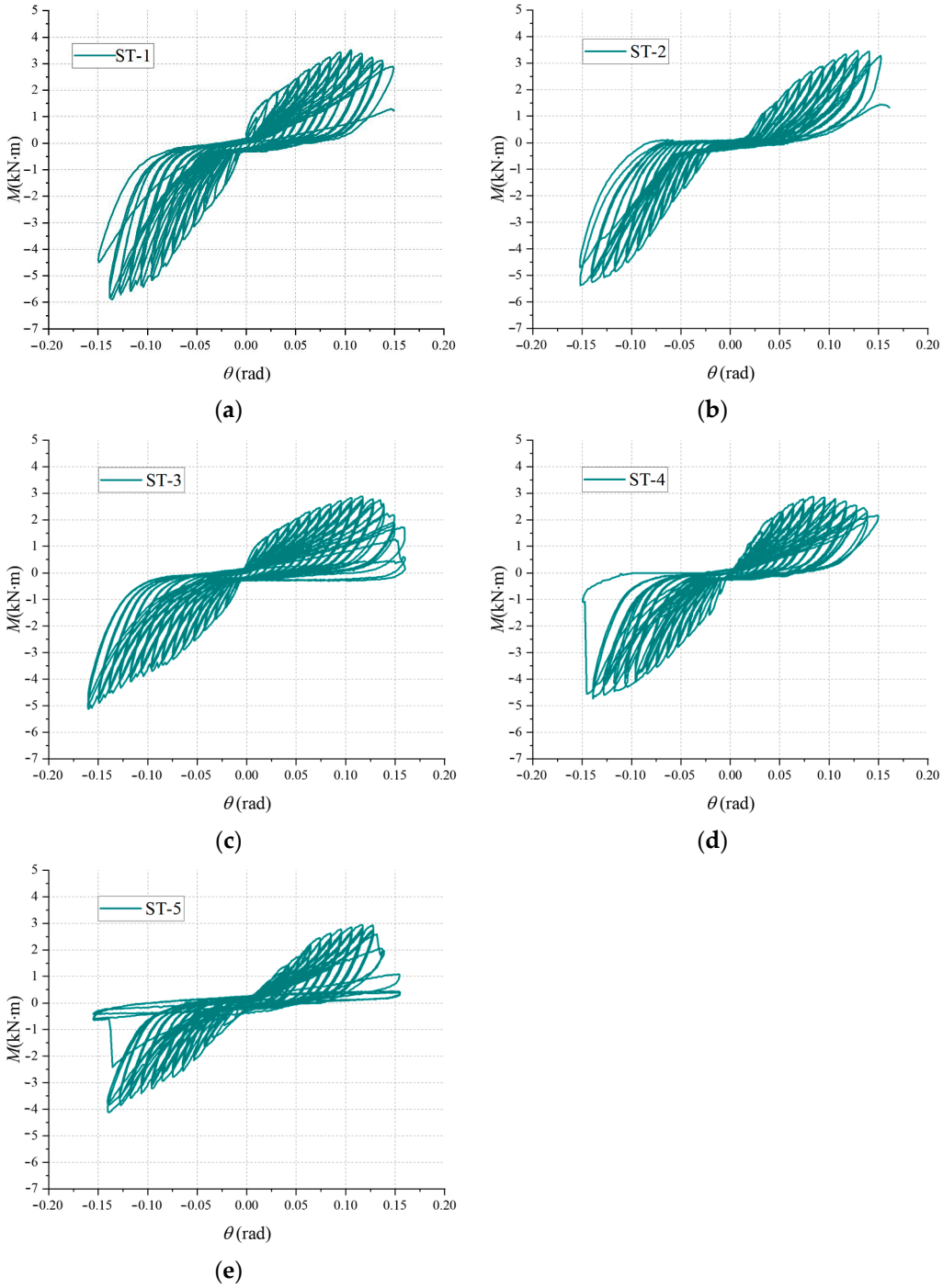


Figure 13. (**a**) Hysteresis curve of specimens not subjected to decay treatment. (**b**) Hysteresis Curve of Decay 6 weeks Specimen. (**c**) Hysteresis Curve of Decay 12 weeks Specimen. (**d**) Hysteresis Curve of Decay 18 weeks Specimen. (**e**) Hysteresis curve of Decay 24 weeks specimen.

By analyzing Figure 13a–e, the following considerations can be drawn:

By comparing the hysteresis curves of each specimen, it is observed that the curves shift from an anti-'S'-type to an anti-'Z'-type. This shift signifies noticeable pinching and slipping phenomena at the nodes, and these effects become more pronounced with an

increasing decay cycle. Beyond a loading angle of 0.03 rad, the hysteresis curve envelope area and bending moment values for the second and third loadings are smaller than those for the first loading at the same angle. Moreover, with a growing decay cycle, the difference between the hysteresis curve area of the second and third loadings and that of the first loading at the same angle becomes more significant. This suggests plastic deformation in the nodes during the loading process, with the degree of deformation becoming increasingly evident as the decay period lengthens. As the decay period increases, the hysteresis curve envelope area becomes less full, the stiffness of HHTMJ gradually degrades, the bending moment decreases rapidly during unloading, and deformation recovery is smaller. The value of the corner at which the node begins to decrease in bearing capacity during positive loading gradually decreases with an increasing decay cycle. Cracking initiates at the tenon joint during the intermediate stage of loading. As the load advances, the bending moment at the joint progressively diminishes in the forward direction, and the rate of decline in the bending moment decelerates when subjected to negative loading. During this phase, the rotational bending moment of the tenon joint predominantly originates from the transverse compression applied by the compressive side of the tenon diameter and the compression of the tenon shoulder against the column. Nevertheless, as the loading displacement increases, cracks multiply, causing a gradual decrease in the bending moment at the joint, ultimately culminating in failure.

Figure 14 illustrates the skeleton curve of HHTMJ. Initially, in the pre-loading phase, the positive and negative loading moment values of the skeleton curve exhibit symmetry. As the loading displacement increases, noticeable asymmetry appears in the skeleton curve, with the negative loading bending moment significantly surpassing the positive loading. This asymmetry arises because, during substantial negative loading, the tenon shoulder slightly elevates the head of the column. This positioning subjects the column's head to the influence of the wood pad at the top and axial pressure constraints, resulting in increased stiffness of the HHTMJ during negative rotation.

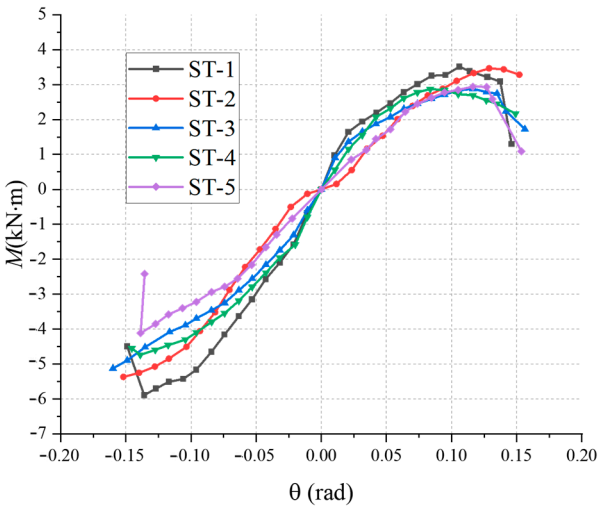


Figure 14. Skeleton curve.

The skeleton curve of HHTMJ can be categorized into elastic, plastic strengthening, and destruction phases. Initially, during the early loading stage, the primary force mode between nodes involves extrusion between mortise side edges and tenons, causing a faster growth of bending moments in the elastic stage. It is observed that, with an increase in the decay cycle, the elastic stage constitutes a smaller proportion of the overall loading stage. As loading continues, the rate of bending moment growth at the joint decreases, and the tenon undergoes significant deformation, entering the plastic strengthening stage. When comparing the plastic strengthening stages of different decayed joint specimens, it is noted that post-decay, the slope of the skeleton curve in this stage decreases significantly,

accompanied by an increase in joint plastic deformation. Towards the end of the plastic strengthening stage, tenon cracking results in a gradual decrease in bearing capacity, marking the entry into the damage stage. As the decay cycle increases, the loading angle at the beginning of the damage stage gradually decreases, and the curve's decline in this stage becomes more pronounced. A higher degree of decay increases the likelihood and severity of node damage at the same loading level. Taking the ultimate bearing load of the ST-1 node during negative loading as a reference, specimens ST-2, ST-3, ST-4, and ST-5 degraded by 8.83%, 16.97%, 19.69%, and 30.22%, respectively.

3.3. Strength and Stiffness Degradation

At the same loading level, the peak load and hysteresis loop area are larger in cycle 1, indicating that the HHTMJ undergoes plastic deformation in cycle 1, resulting in voids between the tenons in cycles 2 and 3. In the proposed horizontal static loading test, three cycles of loading were carried out for each loading stage, and the horizontal load acting on the joints gradually decreased with an increase in loading times. The strength degradation factor can be calculated using the following equation:

$$\lambda_i = \frac{P_{i,3}}{P_{i,1}} \tag{3}$$

where λ_i is the strength degradation factor of the i-th loading level; $P_{i,1}$ is the peak load value of the first cycle in the i-th loading level, and $P_{i,3}$ is the peak load value of the third cycle in the i-th loading level. The variation rule of the strength degradation factor of each node calculated by Equation (3) is shown in Figure 15 below.

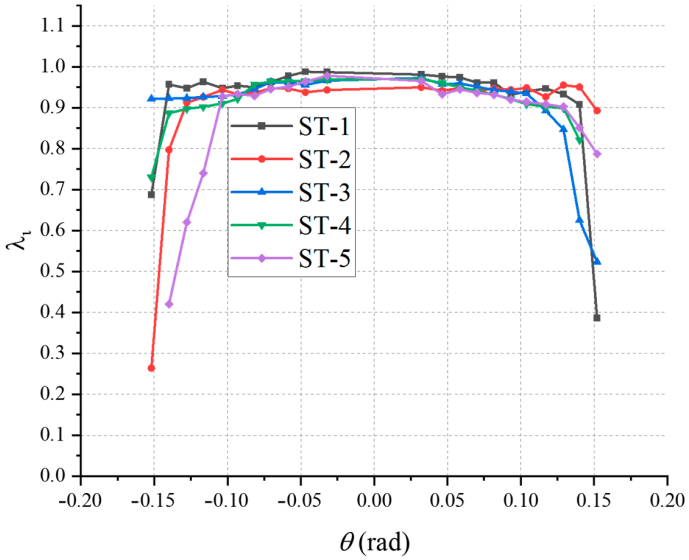


Figure 15. Strength degradation.

The phenomenon of a gradual reduction in stiffness with an increase in the number of loading cycles and displacements is called stiffness degradation. Stiffness can be expressed by the cut-line stiffness of the hysteresis curve under all levels of loading displacements in the presence of horizontal repeated loading, using the following calculation formula:

$$K_{\pm i} = \frac{|M_{\pm i}|}{|\theta_{\pm i}|} \tag{4}$$

where K_i is the cut line stiffness under the action of the loading displacement of the i-th level; M_i is the peak point bending moment under the action of the loading displacement of the i-th level; θ_i is the node turning angle corresponding to M_i. The rotational stiffness of each node is calculated by Equation (4), as shown in Figure 16.

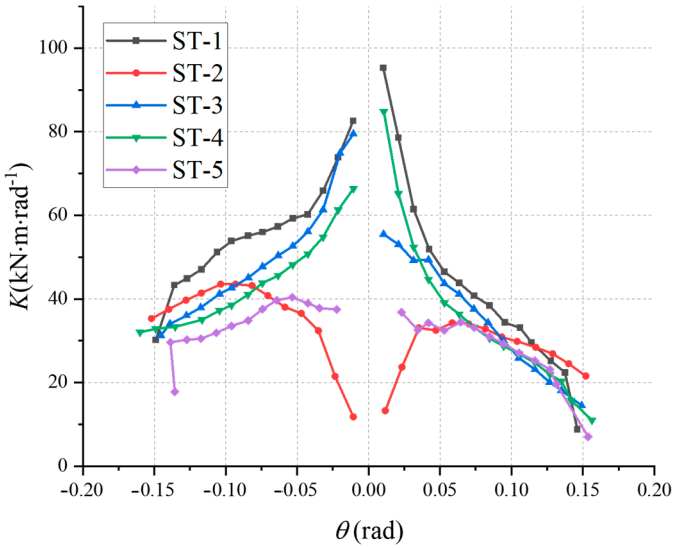


Figure 16. Stiffness degradation.

As depicted in Figure 15, the strength degradation curves for each specimen follow a similar pattern. Generally, a more pronounced strength degradation is observed with an increasing number of decay cycles. Before a loading angle of 0.10 rad, the strength degradation factor for all specimens remains above 0.9, signifying that even under smaller loads, the specimens retain a certain level of strength. The strength degradation factor gradually decreases in each specimen as loading displacement increases, with a more significant decline corresponding to higher decay cycles. Under larger loads, specimens with greater decay cycles exhibit a smaller strength degradation factor compared to those with smaller decay cycles. From the loading corner to the initiation of node damage, specimens with a longer decay period experience a more pronounced decrease in the strength degradation factor than specimens with a shorter decay period. This suggests that as the degree of decay in the HHTMJ increases, the specimen's ability to recover from deformation significantly diminishes at the same loading level. Moreover, the specimen's strength experiences a more rapid decline in the damage stage, leading to a substantial decrease in its ability to withstand larger loads.

Presented in Figure 16, the overall trend indicates a gradual reduction in the stiffness degradation of all specimens as the loading level increases. Notably, the stiffness during the positive loading stage proved to be smaller than that in the negative loading stage. Specimen ST-2 features lower specimen stiffness in the preloading stage due to an initial gap. For the remaining specimens, specimen stiffness exhibited an inverse relationship with the decay cycle. Specifically, in comparison to specimen ST-1, specimen ST-5 displayed an initial stiffness degradation of approximately 54.4% in the positive loading stage and 55.7% in the negative loading stage. The specimens experienced a swift decrease in stiffness during the pre-loading stage, with the rate slowing down post-loading to the plastic strengthening stage. Throughout the damage stage, the rate of stiffness degradation escalated, marked by a sudden drop when the specimen suffered more extensive damage. At equivalent loading levels, specimen stiffness decreased with larger decay cycles, and the decrease was more rapid for higher loading levels.

3.4. Energy Dissipation Capacity Degradation

3.4.1. Energy Dissipation Capacity Degradation

The energy dissipation capacity of the HHTMJ is indicated by the envelope area of the hysteresis curve, and the cumulative energy dissipation (E_c) for the experiment's mortise-tenon joint is obtained by summing the hysteresis curve's area [43]. The results for the cumulative energy dissipation coefficient of the HHTMJ are depicted in Figure 17 through the calculation of the envelope area of the hysteresis curve. Examination of the

figure reveals that, during the pre-loading period, the cumulative energy dissipation of each specimen increases gradually, with the cumulative energy dissipation values for positive and negative loading being essentially symmetrical. With an increase in loading displacement, joint energy dissipation accelerates, reaching its maximum value when loading leads to specimen destruction. In comparison to specimen ST-1, specimens ST-2, ST-3, ST-4, and ST-5 exhibit a decrease in cumulative energy dissipation by 21.6%, 27.4%, 33.2%, and 41.3%, respectively. The occurrence of decay has a more significant impact on the cumulative energy performance degradation of the HHTMJ, while the increase in the degree of decay has a comparatively smaller effect on the cumulative energy performance degradation of the HHTMJ.

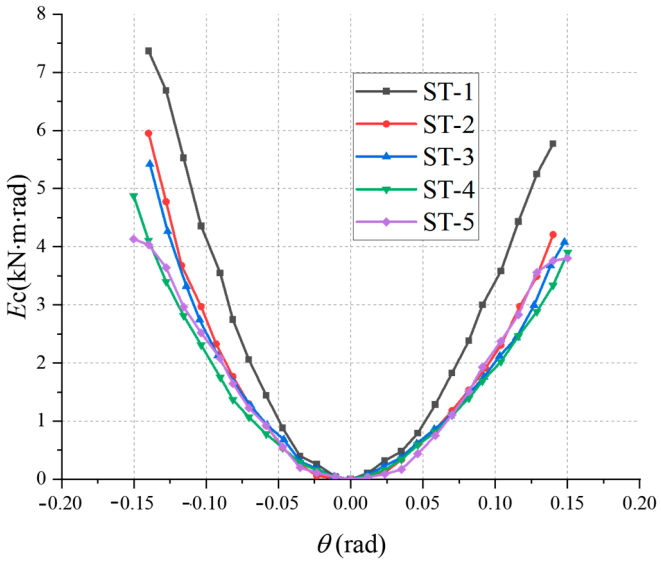


Figure 17. Accumulated energy consumption degradation.

3.4.2. Energy Dissipation Degradation

The energy dissipation performance of a joint is expressed using the dimensionless equivalent viscous damping factor E_{dc} [44], the larger the value of E_{dc}, the stronger the energy dissipation performance of the joint. The schematic diagram of the calculation method is shown in Figure 18, and the calculation formula is as follows:

$$E^{+}{}_{dc} = \frac{1}{2\pi} \cdot \frac{S_{ABC}}{S_{\Delta BFO}}; E^{-}{}_{dc} = \frac{1}{2\pi} \cdot \frac{S_{ADG}}{S_{\Delta DEO}} \quad (5)$$

In the formula, E is the energy dissipation coefficient; S_{ABC} and S_{ADG} are the envelope area of the hysteresis curve, which is the shaded area in Figure 18; $S_{\Delta DEO}$ is the area of Δ_{DEO}, and $S_{\Delta DEO}$ is the area of Δ_{BFO}, which is the ideal elastic energy dissipation performance of HHMTJ.

Figure 19 illustrates the energy dissipation coefficients for the first cycle at various loading displacement levels of the specimen, with a similar trend observed in the viscous damping coefficients of all specimens. During the pre-loading phase, there is minimal tenon slip and pullout, resulting in superior energy dissipation performance. With increasing loading displacement, the slip between the tenon and mortise grows, and the rise in extrusion deformation between them during the slip process is less pronounced, leading to a decrease in energy dissipation performance. In the destructive stage, there is a sharp increase in extrusion deformation between the tenon and mortise, enhancing the specimen's capacity for dissipation. Beyond a loading turn angle of 0.02 rad, the changes in the curve for negative loading become more consistent, attributed to the complexity of tenon slip, extrusion deformation, and damage in positive loading.

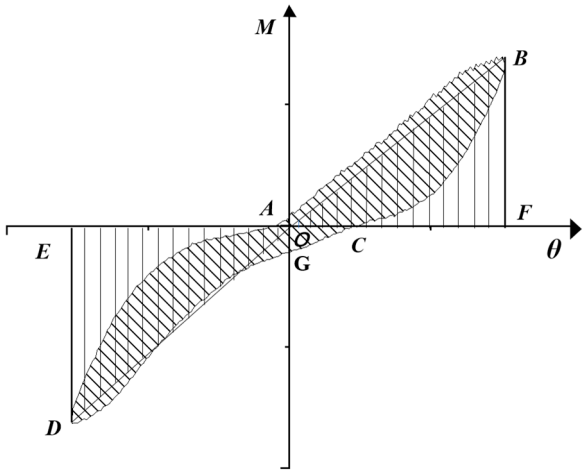


Figure 18. Definition of equivalent viscous damping ratio for one cycle.

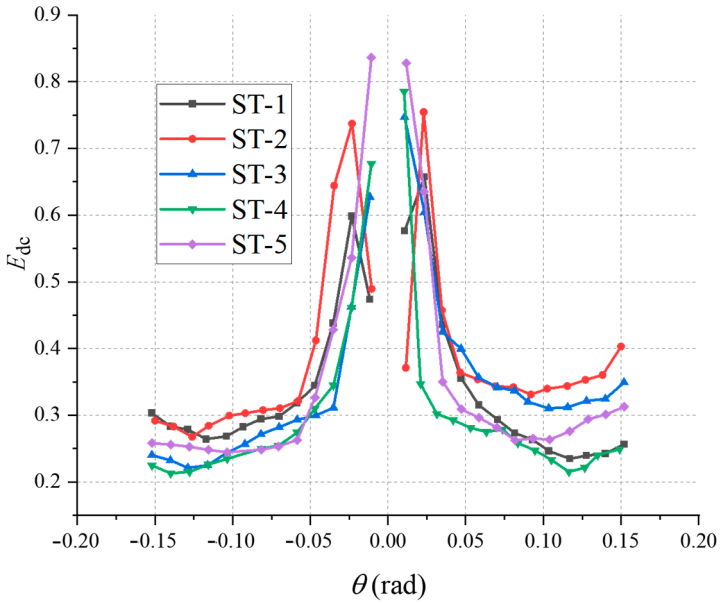


Figure 19. Energy consumption performance degradation.

In comparison to specimen ST-1, the energy dissipation coefficient is higher during the pre-loading period for the specimen with decay, but it decreases more rapidly as loading displacement increases, especially for specimens with larger decay cycles. This phenomenon is attributed to increased friction between the tenon and mortise after HHTMJ decay, allowing the mortise and tenon to undergo some extrusion deformation during the pre-loading phase, thereby enhancing energy dissipation. As loading displacement rises, tenon slip occurs, leading to a decrease in joint extrusion deformation and a rapid decline in HHTMJ energy dissipation performance. In the destructive stage, the capacity dissipation coefficient experiences a slight increase, with a more noticeable rise for specimens with larger decay cycles. This increase is due to the initiation of plastic deformation and destruction in the HHTMJ as the decay cycle grows. In general, decay and small external loads make the tenon more susceptible to slip, plastic deformation, and damage, thereby diminishing the energy dissipation capacity of the specimens. Nevertheless, after decay, the HHTMJ can still retain a certain energy dissipation capacity under low weekly repeated loads, signifying a positive impact on resistance to seismic impact loads. This is the reason why many Tusi Manor structures in Tibetan areas of Yunnan can withstand various earthquakes over an extended period of time.

3.5. Degradation of HHTMJ Rotation Capacity

According to the provisions in the Technical Standard for Maintenance and Reinforcement of Wooden Structures of Ancient Buildings (GB/50165-2020) [45], the limit value of the interstorey displacement angle of the wooden structure building is 1/30. In the Tusi Manor in Tibetan areas in Yunnan, the deformation of the internal wooden frame is mainly caused by the deformation of the mortise and tenon nodes, and it can be regarded as the limit value of the rotational performance of the hoop-and-tenon nodes of 1/30. As can be seen from Figure 13, the node bending moment of specimen ST-5 still rises when the loading angle is 0.12 rad (about 1/8), which indicates that the HHTMJ with decay still has a good rotational performance.

4. The Impact of Mechanical Performance Degradation on the Seismic Degradation of HHTMJ

The degradation data for wood mechanical properties in Figures 20 and 21 are extracted from the results in Table 1. E_c represents the maximum cumulative energy dissipation degradation rate, while ML represents the rate of ultimate bearing capacity performance degradation. Figure 20 illustrates a comparison of seismic performance degradation data between small-size transverse compressive specimens subjected to decay treatment, HHTMJ specimens, and transverse compressive specimens sawn from the tenon with HHTMJ specimens. As shown in Figure 20, the degradation level of small-size transverse grain specimens falls between the cumulative energy dissipation of HHTMJ and the degradation level of ultimate bearing performance, with the degradation levels of these three aspects being relatively close. However, the degradation level of transverse grain specimens obtained from the tenon exterior is less than the preceding three, approaching half of their degradation levels. When comparing the degradation levels of transverse compression strength specimens from the inside and outside of the tenon, it becomes evident that there is almost no decay occurring inside the tenon. It is evident that when the tenon undergoes slight decay, the seismic performance of HHTMJ shows significant degradation, with the degree of degradation being approximately twice that of the transverse compressive strength specimens outside the tenon.

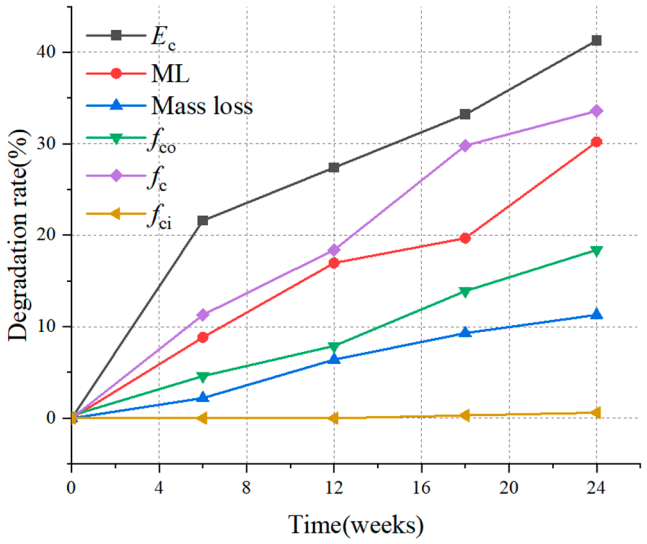


Figure 20. Relationship of compressive stress perpendicular to grain and seismic performance.

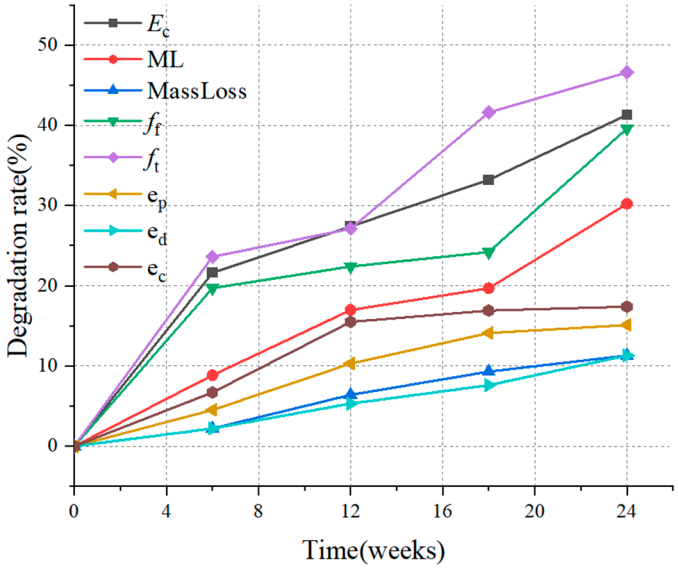


Figure 21. Relationship between mechanical properties and seismic degradation of small-sized specimens.

By comparing the degradation level of seismic performance in HHTMJ with the degradation of tensile strength, bending strength, and compressive modulus of elasticity in longitudinal wood, as shown in Figure 21, the performance of HHTMJ under low-cycle repeated loading can be explained. Within the same decay period, the longitudinal tensile strength of the HHTMJ experiences the most significant decrease. Moreover, as the specimens reach the same rotation angle, the longer the decay period, the more pronounced the increase in cracking at the tension end of the tenon shoulder upon specimen failure. The degradation of bending strength along the grain of wood closely corresponds to the degradation curve of the ultimate load-carrying performance of HHTMJ. This is because the nodal bending moment is primarily supplied by the bending force acting on the wood along the grain direction at the tenon shoulder. Compared to the degradation of other mechanical properties, the degradation of the elastic modulus is relatively small. This is also the reason why the deformation of the tenon and mortise of HHTMJ is minimal after being subjected to force. In the context of Tusi Manor in Tibetan areas in Yunnan, obtaining a comprehensive assessment of HHTMJ is relatively challenging. However, acquiring smaller-sized specimens for testing the mechanical performance of wood is feasible. Based on the previous analysis, the degree of mechanical performance degradation in wooden components outside the tenon is closely correlated with the deterioration of HHTMJ seismic performance. This holds a certain reference value.

5. Conclusions

Decay disease has a serious impact on traditional buildings with historical and cultural values, and it is of positive significance to assess the impact of decay disease on the durability of such buildings and then propose feasible improvement measures to protect such buildings. In this paper, through five cycles of decay treatment on the HHTMJ of the Tusi Manor in Tibetan areas in Yunnan and low-cycle loading and mechanical properties test experiments, according to the experimental results of the HHTMJ seismic performance degradation and the reasons for the analysis, the following conclusions were obtained:

(1) Under the action of low-cycle repeated loading, the damage to HHTMJ occurs mainly in the connection area of tenon and mortise, plastic deformation and fracture of tenon at the shoulder of tenon, and plastic deformation and splitting damage of wood in the contact area between the outside of tenon and the shoulder of tenon. The longer the decay period, the greater the extent of damage to the HHTMJ under the same level of loading. Additionally, more wood chips will detach along the direction of the wood

grain at the upper end of the tenon shoulder. Simultaneously, the failure mechanism of HHTMJ during the stress process becomes more intricate.

(2) As the decay cycle increases, the hysteresis curve of the HHTMJ transitions from anti-"S"-type to anti-"Z"-type, and the hysteresis curve becomes less and less full. The elastic loading stage of the skeleton curve decreases, the plastic strengthening stage increases, and the strength and stiffness of the HHMTJ degrade obviously under external force. Compared with the undecayed specimens, the ultimate load-carrying capacity of the HHTMJ decreased by 8.83%, 16.97%, 19.69%, and 30.22% for 6, 12, 18, and 24 weeks of decay, respectively, and the cumulative energy dissipation decreased by 21.6%, 27.4%, 33.2%, and 41.3%, respectively.

(3) The extent of degradation in the transverse compressive strength of wood, treated for decay alongside HHTMJ, closely correlates with the deterioration in HHTMJ seismic performance. Meanwhile, the degradation in the transverse compressive strength of wood taken from decayed tenon joints is roughly half of that observed in the former two cases. Specimens extracted from the decayed tenon interior show little to no degradation, which is also the main reason why decayed HHHMJ maintains a certain level of rotational capability. When evaluating the seismic performance of decayed HHTMJ in ancient buildings, the difference in transverse compressive strength between the interior and exterior woods of tenon can be indirectly used to assess the seismic performance of HHTMJ.

Author Contributions: Z.N. contributed to the investigation, experiments, experimental analysis, and manuscript; H.L. contributed to the Investigation, experiments, and image processing; K.W. contributed to the investigation; M.Y. contributed to the experimental analysis. Z.Y. provided suggestions for revising the manuscript. Y.S. contributed to the conceptualization and methodology. M.Q. contributed to the funding acquisition, supervision, and manuscript revision. All authors have read and agreed to the published version of the manuscript.

Funding: This research was funded by "Joint Agricultural Project in Yunnan Province, China", grant number "202101BD070001-097"; "Open Fund Project of National Local Joint Engineering Re-search Center", grant number."2023-GC02"; "Study on the Mechanical Performance of Typical Nodes in Dam-aged Ancient Wooden Structures", grant number "10822037"; 111 Project grant number "D21027".

Data Availability Statement: The data is designed to be used in other ongoing research and should be protected before official publication.

Conflicts of Interest: The authors declare no conflicts of interests.

References

1. Qi, Y.T. *Protection and Maintenance of Ancient Chinese Architecture*; Cultural Relics Publishing House: Beijing, China, 1986. (In Chinese)
2. Dong, J.; Jin, H. The design strategy of green rural housing of Tibetan areas in Yunnan, China. *Sel. Pap. World Renew. Energy Congr.—XI* **2013**, *49*, 63–67. [CrossRef]
3. Brischke, C.; Bayerbach, R.; Rapp, A.O. Decay-influencing factors: A basis for service life prediction of wood and wood-based products. *Wood Mater. Sci. Eng.* **2006**, *1*, 91–107. [CrossRef]
4. Taylor, A.; Lloyd, J.; Shelton, T. An open letter to proponents of CLT/Massive Timber. In Proceedings of the IRG Annual Meeting, Lisbon, Portugal, 15–19 May 2016; p. 7.
5. Qin, S.; Yang, N. Strength Degradation and Service Life Prediction of Timber in Ancient Tibetan Building. *Eur. J. Wood Wood Prod.* **2018**, *76*, 731–747. [CrossRef]
6. Yang, N.; Jia, Y.T.; Bai, F.; Qin, S.J. Reliability estimation of a Tibetan heritage timber structure with inclination in its Que-Ti joints. *Structures* **2022**, *43*, 257–270. [CrossRef]
7. Chen, Q.; He, Y.; Qiu, K.; Tang, X.; Cai, J.; Yang, C. Theoretical Analysis of Moment Rotation Relationship of Hoop Joint in Guangfu Ancient Architecture Wood Structure. *J. Hunan Univ. (Nat. Sci. Ed.)* **2019**, *46*, 65–75. (In Chinese) [CrossRef]
8. Zhang, B.; Xie, Q.; Liu, Y.; Zhang, L.; Li, S. Effects of gaps on the seismic performance of traditional timber frames with straight mortise-tenon joint: Experimental tests, energy dissipation mechanism and hysteretic model. *J. Build. Eng.* **2022**, *58*, 105019. [CrossRef]

9. Bai, F.; Dong, F.; Sui, Y.; Xue, J.; Wu, C.; Song, D.; Hu, C. Experimental study on fracture damage and seismic performance of loose through-tenon joints in ancient timber structures. *Constr. Build. Mater.* **2023**, *394*, 132228. [CrossRef]
10. He, J.; Yu, P.; Wang, J.; Yang, Q.; Han, M.; Xie, L. Theoretical model of bending moment for the penetrated mortise-tenon joint involving gaps in traditional timber structure. *J. Build. Eng.* **2021**, *42*, 103102. [CrossRef]
11. Yang, Q.; Yu, P.; Law, S.-S. Load resisting mechanism of the mortise-tenon connection with gaps under in-plane forces and moments. *Eng. Struct.* **2020**, *219*, 110755. [CrossRef]
12. King, W.S.; Yen, J.Y.R.; Yen, Y.N.A. Joint characteristics of traditional Chinese wooden frames. *Eng. Struct.* **1996**, *18*, 635–644. [CrossRef]
13. Chen, L.-K.; Li, S.-C.; King, W.-S.; Jiang, L.-Z.; Luo, H.-Z.; Li, Q.-J. How the decayed straight mortise-tenon joints influence the seismic performance of ancient timber building? Evidence from experiment scenarios of the benchmark wood frames. *Eng. Fail. Anal.* **2020**, *116*, 104685. [CrossRef]
14. Chang, P.; Feng, Q.; Han, L.; Yang, N. Experimental Study on Seismic Performance of Hoop Joint under Loose Damage. *J. Build. Struct.* **2023**, *44*, 86–96. (In Chinese) [CrossRef]
15. Chen, Q.; Peng, Z.; Cai, J.; Huang, C.; Tang, X.; Qiu, K.; Yang, C. Research on seismic performance of wooden structure hooped tenon joints in Guangfu ancient architecture. *J. Build. Struct.* **2019**, *40*, 168–179. (In Chinese) [CrossRef]
16. Venäläinen, M.; Partanen, H.; Harju, A. The strength loss of Scots pine timber in an accelerated soil contact test. *Int. Biodeterior. Biodegrad.* **2014**, *86*, 150–152. [CrossRef]
17. Kleindienst, Q.; Besserer, A.; Antoine, M.-L.; Perrin, C.; Bocquet, J.-F.; Bléron, L. Predicting the beech wood decay and strength loss in-ground. *Int. Biodeterior. Biodegrad.* **2017**, *123*, 96–105. [CrossRef]
18. Plaschkies, K.; Jacobs, K.; Scheiding, W.; Melcher, E. Investigations on natural durability of important European wood species against wood decay fungi; Part 1: Laboratory tests. *Int. Biodeterior. Biodegrad.* **2014**, *90*, 52–56. [CrossRef]
19. Ueda, R.; Sawata, K.; Takanashi, R.; Sasaki, Y.; Sasaki, T. Degradation of Shear Performance of Screwed Joints Caused by Wood Decay. *J. Wood Sci.* **2020**, *66*, 42. [CrossRef]
20. Li, S.; Gao, Y.; Brunetti, M.; Macchioni, N.; Nocetti, M.; Palanti, S. Mechanical and physical properties of *Cunninghamia lanceolata* wood decayed by brown rot. *Iforest Biogeosci. For.* **2019**, *12*, 317–322. [CrossRef]
21. Wang, X.; Xu, Q.; Wang, X.; Guo, J.; Cao, W.; Xiao, C. Strength degradation of wood members based on the correlation of natural and accelerated decay experiments. *J. Renew. Mater.* **2020**, *8*, 565–577. [CrossRef]
22. Conde-García, M.; Tenorio-Ríos, J.A.; Fernández-Golfín, J. Experimental evaluation of the effect of different design conditions on the risk of decay in solid wood exposed to outdoor climate. *Mater. Construcción* **2021**, *71*, e247. [CrossRef]
23. Mi, X.; Li, Y.; Qin, X.; Li, J. Effects of Natural Weathering on Aged Wood from Historic Wooden Building: Diagnosis of the Oxidative Degradation. *Herit. Sci.* **2023**, *11*, 109. [CrossRef]
24. Bažant, Z.P.; Yavari, A. Is the Cause of Size Effect on Structural Strength Fractal or Energetic–Statistical? *Eng. Fract. Mech.* **2005**, *72*, 1–31. [CrossRef]
25. Kim, G.-H.; Barnes, H.M.; Lyon, D.E. Effect of Decay on the Mechanical Properties of Full-Sized Lum-ber. *Holzforschung* **1994**, *48*, 145–149. [CrossRef]
26. Panoutsopoulou, L.; Mouzakis, C. Experimental investigation of the behavior of traditional timber mortise-tenon T-joints under monotonic and cyclic loading. *Constr. Build. Mater.* **2022**, *348*, 128655. [CrossRef]
27. Zhang, C.; Chun, Q.; Lin, Y.; Han, Y.; Jia, X. Quantitative assessment method of structural safety for complex timber structures with decay diseases. *J. Build. Eng.* **2021**, *44*, 103355. [CrossRef]
28. Udele, K.E.; Morrell, J.J.; Cappellazzi, J.; Sinha, A. Characterizing properties of fungal-decayed cross laminated timber (CLT) connection assemblies. *Constr. Build. Mater.* **2023**, *409*, 134080. [CrossRef]
29. Ma, L.; Xue, J.; Zhang, X. Seismic Performance Evaluation of Damaged Ancient Timber Structures with Looseness Mortise-Tenon Joints. *Int. J. Archit. Herit.* **2023**, *17*, 2054–2068. [CrossRef]
30. Chen, L.; Li, S.; Wang, Y.; Zhao, Y.; Zhang, M.; Song, X.; Li, X.; Wu, T.; Jiang, L. Experimental Study on the Seismic Behaviour of Mortise–Tenon Joints of the Ancient Timbers. *Struct. Eng. Int.* **2017**, *27*, 512–519. [CrossRef]
31. *GB/T 1927.2-2021*; Test Methods for Physical and Mechanical Properties of Small Clear Wood Specimens—Part 2: Sampling Methods and General Requirements. Standardization Administration of the People's Republic of China: Beijing, China, 2021. (In Chinese)
32. *GB/T 1927.10-2021*; Test Methods for Physical and Mechanical Properties of Small Clear Wood Specimens—Part 10: Determination of Modulus of Elasticity in Bending. Standardization Administration of the People's Republic of China: Beijing, China, 2021. (In Chinese)
33. *GB/T 1927.13-2022*; Test Methods for Physical and Mechanical Properties of Small Clear Wood Specimens—Part 13: Determination of the Modulus of Elasticity in Compression Perpendicular to Grain. Standardization Administra-tion of the People's Republic of China: Beijing, China, 2022. (In Chinese)
34. *GB/T 15777-2017*; Method for Determination of the Modulus of Elasticity in Compression Parallel to Grain of Wood. Standardization Administration of the People's Republic of China: Beijing, China, 2017. (In Chinese)
35. Liang, W.; Lan, J.; Zou, Z.; Zhu, Z.; Zhai, S.; Mo, Y.; Li, X.; Meng, S.; Cai, Y. Seismic behavior of Chuan-dou timber frames with different infilled walls. *Constr. Build. Mater.* **2022**, *327*, 126906. [CrossRef]

36. Ma, L.; Xue, J.; Dai, W.; Zhang, X.; Zhao, X. Moment-rotation relationship of mortise-through-tenon connections in historic timber structures. *Constr. Build. Mater.* **2020**, *232*, 117285. [CrossRef]
37. Hu, L.; Liu, L.; Wang, G.; Wu, J. Identification of decaying fungi on beams and columns of buildings in the Old Town of Lijiang. *Mycol. Res.* **2016**, *14*, 153–156. (In Chinese) [CrossRef]
38. *GB/T 13942.1-2009*; Forestry RIoWICAo, Durability of Wood—Part. 1: Method for Laboratory Test of Natural Decay Resistance, General Administration of Quality Supervision, Inspection and Quarantine of the People's Republic of China. Standardization Administration of the People's Republic of China: Beijing, China, 2009; p. 12. (In Chinese)
39. Yang, Z.; Jiang, Z.; Reng, H.; Qin, D. An Accelerated Laboratory Test Method to Assess Wood Decay. *China Wood Ind.* **2007**, *04*, 12–14+20. (In Chinese) [CrossRef]
40. Bouslimi, B.; Koubaa, A.; Bergeron, Y. Effects of biodegradation by brown-rot decay on selected wood properties in eastern white cedar (*Thuja occidentalis* L.). *Int. Biodeterior. Biodegrad.* **2014**, *87*, 87–98. [CrossRef]
41. *ASTM D2017-05*; Standard Method of Accelerated Laboratory Test of Natural Decay Resistance of Wood. American Society for Testing and Materials: West Conshohocken, PA, USA, 2008.
42. *JGJ 101-2015*; Specification of Test Methods for Earthquake Resistant Building. China Academy of Building Research: Beijing, China, 1996.
43. Lacourt, P.A.; Crisafulli, F.J.; Mirasso, A.E. Finite element modelling of hysteresis, degradation and failure of dowel type timber joints. *Eng. Struct.* **2016**, *123*, 89–96. [CrossRef]
44. *EN 12512:2001*; Timber Structures-Test Methods-Cyclic Testing of Joints Made with Mechanical Fasteners. European Committee for Standardization: Bruxelles, Belgium, 2001.
45. *GB 50165-1992*; National Technical Committee for Timber and Composite Materials Standards, Technical Code for Maintenance and Strengthing of Ancient Timber Buildings. Sichuan Institute of Building Research: Chengdu, China, 1992.

Disclaimer/Publisher's Note: The statements, opinions and data contained in all publications are solely those of the individual author(s) and contributor(s) and not of MDPI and/or the editor(s). MDPI and/or the editor(s) disclaim responsibility for any injury to people or property resulting from any ideas, methods, instructions or products referred to in the content.